Response to Reviewer Comment

We sincerely appreciate the reviewer's thorough assessment of our manuscript and their constructive comments. Below we provide a detailed response to each of the major and minor comments.

Major Comment 1: Reflection Height Assessment

The assessment of reflection height is improved from the previous version of this paper, but it still appears to be incorrect. The measurement of the first cutoff frequency altitude, as shown in Figure 1, is sufficient. But the model-derived reflection height (section 2.4) is problematic. The model provides an electron density (as in Figure 2); the authors then fit a Wait and Spies profile (equation 2) to the model D-region profile. They extract h', the Wait parameter, and use that as the reflection height. But, as I noted in the GRL review, h' is not the reflection height; it is merely a reference height for the electron density profile. The reflection height is correctly described in the paper as the height where X = Z in the Ratcliffe formulation, or wp^2 = w*nu (equation 3, except a factor of 2*pi is missing).

The next steps in the paper are confusing. The authors use the first waveguide cutoff frequency from the ELF data, plug that into equation 3, and then solve for h'... But they already assumed a reflection height from the cutoff frequency through f = c/h' for the cutoff frequency. This circular logic is confusing, and it is not clear (and not stated) which h' is used in the rest of the paper.

The assessment of the reflection height from the model can be made much simpler. Use the electron density from the model to calculate wp^2. Use equation 4 to calculate nu, the collision frequency profile. Now, you can plot X/Z as a function of altitude (on the y-axis) and frequency (on the x-axis), just as Ratcliffe did in his book. For the frequency of interest (say, the f1 determined from the ELF data), you can find the altitude where that frequency reflects.

The authors should still point out that for ELF/VLF frequencies, this is not a hard reflection; it occurs over a range of 5-10 km in altitude. But it is true that a lower effective reflection height is consistent with precipitation, as shown in Marshall and Cully [2020].

We thank the reviewer for this suggestion. We have calculated the reflection height exactly following your suggestion. We first used equation 4 to calculate the collision frequency ν at different heights z, and the plasma frequency f_p at those heights was calculated using the model's electron density. These two parameters were then substituted into the equation $f_p^2=f_1\nu$, leading to the relationship between different wave frequencies and their reflection heights (equation 6). We then used the observed f_1 from the EFD payload and equation 6 in order to obtain the relation between the reflection height h′ and the frequency f_1.

We admit that there was a logical issue in our description, which likely caused confusion regarding the relationship between z and h′. To address this, we have revised section 2.4, providing a clearer distinction between z and h′. Specifically, in line 213, we describe: "when discussing specific reflection heights at a particular frequency, h' will be used". Furthermore, in line 217, we clarify equation 6: "we can obtain the relationship between different wave frequencies and their reflection height." In lines 220-223, we offer a detailed explanation of how the data is obtained and how the reflection height is solved: "In this formulation, Ne

(z) represents the electron density (in cm^{-3}) at reflection height z, obtained from PyGPI5 simulations. The cutoff frequency f_l corresponds to the wave frequency that is reflected at a specific height z. Using equation 6, h′ can be determined by finding the height z at which the calculated cutoff frequency matches the observed f_l from CSES EFD measurements. "

These revisions should clarify the logic and resolve any confusion between z and h′. We greatly appreciate the reviewer's insight, and we believe these changes will enhance the clarity of the manuscript.

We also appreciate the reviewer's suggestion to clarify the nature of ELF/VLF reflections. Following this advice, we have added the following statement in lines 223-224: "For ELF/VLF frequencies, these waves are not reflected at a single altitude, but more likely over a range of 5-10 km around the reflection altitude. However, as pointed out by Marshall and Cully (2020), a reflection height that is lower than typical values was found to be more consistent with energetic electron precipitation." This addition strengthens our interpretation of the observed decrease in reflection height during precipitation events.

Major Comments:

2. X-ray observations: This comment is repeated from my GRL review, since I do not see that it was addressed. X-ray observations are shown, which give a spatial distribution similar to the particle fluxes. But apart from a spatial distribution, and a general amplitude correlation (not shown; a figure would be nice). Furthermore, the energy range of the X-ray observations is concerning. These energies (0.9--35 keV) are going to be dominated by bremsstrahlung from auroral electrons (<50 keV), NOT the relativistic electrons usually associated with EPP. Yet, it is intriguing that the X-ray fluxes seem to peak around L=5, clearly sub-auroral and in the radiation belts. Did the authors filter the data to remove times of auroral precipitation somehow? If so, this should be explained. Then, what were the fluxes of lower-energy precipitation electrons at this time? If lower-energy precipitation (<50 keV) is present, at high fluxes as is typical, then the x-rays may have been produced by those electrons, are we would not expect them to be strongly correlated with the electron fluxes or the reflection height (since those electrons deposit energy above the ELF/VLF reflection heights). But all of this information is missing, so cannot be properly assessed.

Thank you for the helpful comments and suggestions. Our recent paper (Liao et al., 2025) shows that areas with higher nightside bremsstrahlung X-ray rates are found in the outer radiation belt (L>4), the South Atlantic anomaly zone, and the slot region (2<L<3). Additionally, strong X-ray radiation can be observed in regions with an L value of approximately 1.7 and a geographic longitude of 150 to 200 degrees. The areas with high X-ray rates detected by CSES correspond closely to the areas with high-energy particle fluxes observed by CSES satellites (Figure 1 (b, c)). The bremsstrahlung process is extremely inefficient for <50 keV electrons, and it becomes more important for MeV electrons (Berger and Seltzer, 1972; Lehtinen et al., 1999). Moreover, the X-rays generated by hundred-keV to MeV electrons are not necessarily in the same energy range, but mostly in the keV range (Lehtinen et al., 1999; Berger and Seltzer, 1972; Xu and Marshall, 2019). As such, the 0.9-35 keV X-rays measured by CSES are not

necessarily produced by auroral electrons since the bremsstrahlung process for <50 keV electrons is inefficient, but more likely produced by hundred-keV and MeV electrons. Due to the limited energy resolution of CSES, we emphasize that X-rays with energies higher than 35 keV could be recorded by CSES, but cannot properly registered.

This correlation is supported by the simulation conducted by one coauthor of this manuscript (Xu and Marshall, 2019), which indicated that the X-rays detected at satellite altitudes primarily originate from the bremsstrahlung production source region. Although bremsstrahlung process becomes more efficient when the electron energy increase, however the distribution of X-ray rates aligns more closely with the electron flux distribution in the energy range of 100-800 keV (Figure 1 (b)) compared with the electron flux distribution in the energy range of 800 keV-3 MeV (Figure 1 (c)). This conclusion has also been confirmed by the spatial cross-correlation analysis by the calculation of Bivariate Moran's I. Unlike the Pearson or Spearman correlation coefficient, the Bivariate Moran's I consider the effect of spatial location on the correlation. The correlation between X-ray rate and electron flux is strong at 100-800 keV (0.77, p-value < 0.01) and moderate at 800 keV to 3 MeV (0.62, p-value < 0.01). That is because electrons with energies below 800 keV tend to have more precipitation energy backscattered into space, which can be detected by satellites. In contrast, the bremsstrahlung photons produced by MeV electrons are more likely to be emitted forward since they are directed downward into the atmosphere (Xu and Marshall, 2019b). X-rays in the radiation belt, particularly in the range of $2 < L < 3$ from 150° E to 260° E in the northern hemisphere, maybe from lightning-induced electron precipitation (LEP). Another apparent feature is, in the energetic electron flux distribution map for 800 keV to 3 MeV, there is a notable slot region between $2 < L < 3$ in the longitudinal range of 300° E to 360° E (Figure 1 c). This slot region does not appear in the distribution maps for the 100-800 keV range (Figure 1b) since the specific slot region is highly energy dependent (e.g., Voss et al., 1984; Linzmayer et al., 2024).

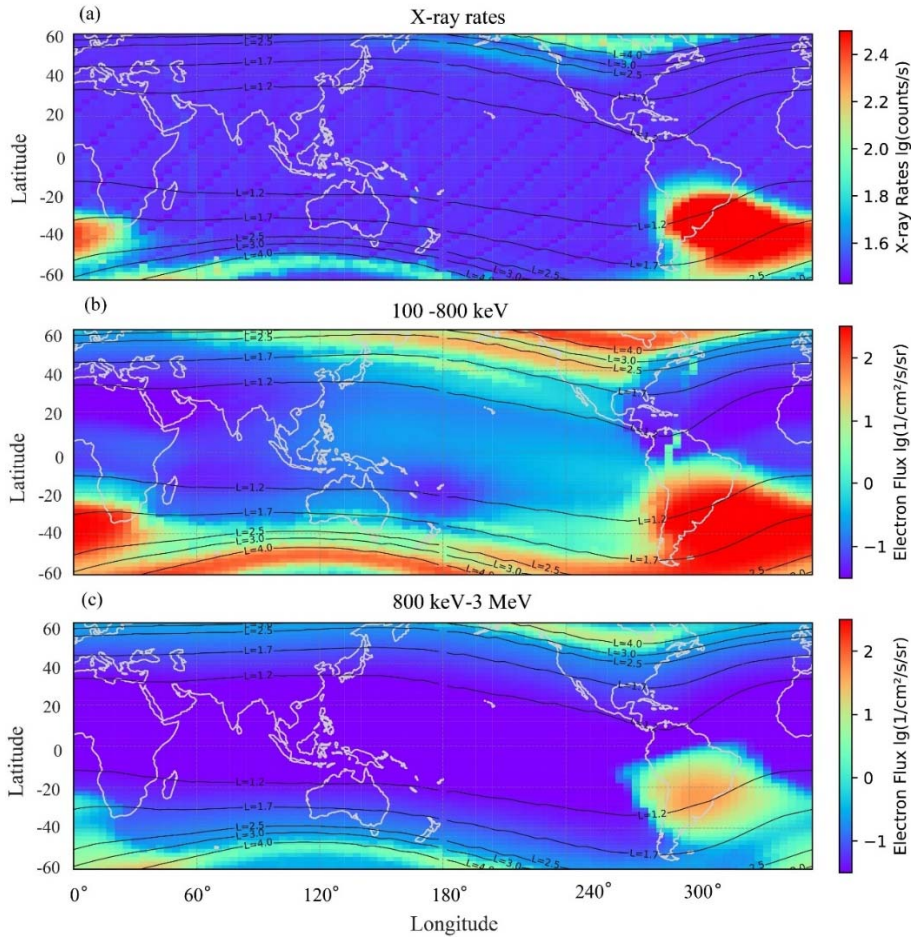

Figure 1.(a) The global nighttime X-ray distributions from 2019 to 2021. (b) The global nighttime electron flux distributions for electrons in the energy range of 100–800 keV from 2019 to 2021. (c) The same format as (b) but for the electrons in the energy range of 800 keV–3 MeV.

From the above results, it can be seen that the night-side X-rays detected by the CSES satellite in the slot region and SAA regions have a low correlation with auroral electrons, which are mainly radiated due to the ionization of the neutral component by electrons in the 100-800 keV range. In the outer radiation belts, as stated by the reviewer, although we currently have no observations that can rule out the influence of auroral electrons (the detection range of CSES satellite electrons in the low-energy band of energy is 100 keV- 3 MeV), the precipitated electrons in the range of 100-800 keV should also play a very important role in the resulting X-ray.

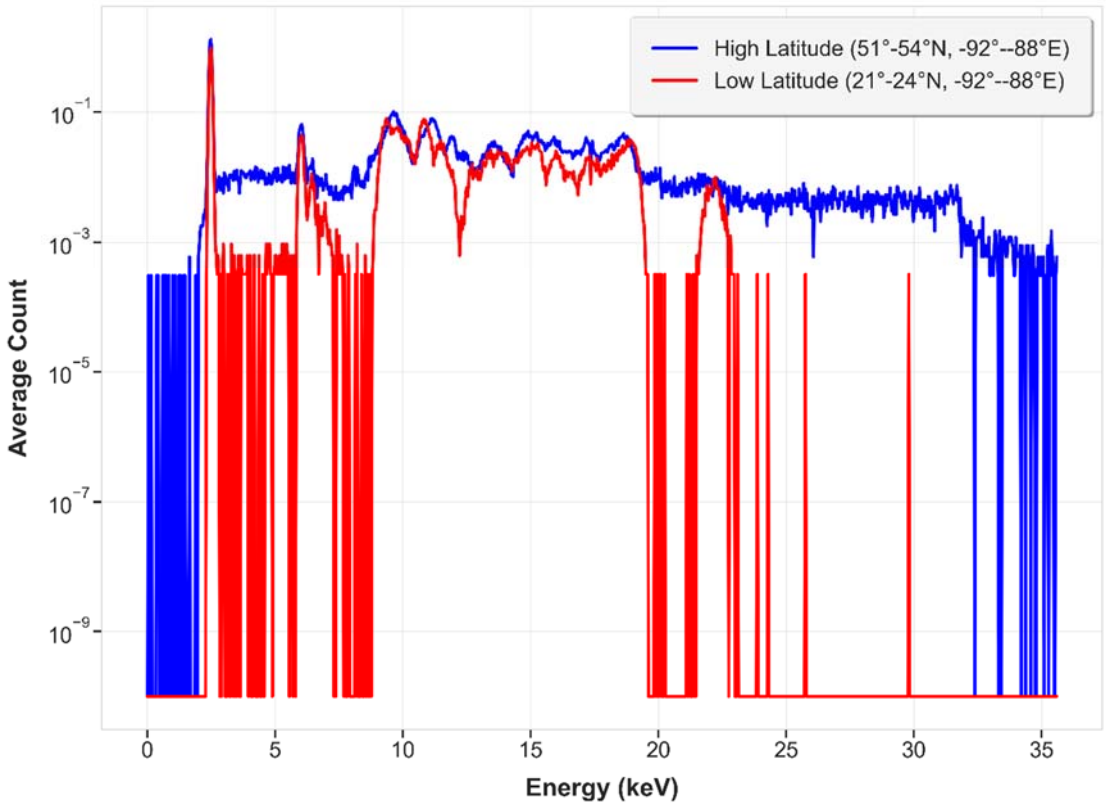

Figure 2. X-ray profiles under different conditions. The figure shows the X-ray distribution in the background condition (red line) and during precipitation condition (blue line), using the average values measured by the CSES-HEPP-X in 2019.

According to the simulation study by Xu et al. (2019), electrons with energies exceeding 100 keV can generate X-rays with energies greater than 10 keV. We conducted a zonal analysis of the CSES satellite data, dividing the observation areas into two categories: high-latitude regions affected by radiation belt electron precipitation and low-latitude regions unaffected by radiation belt electrons. Through an annual average X-ray analysis, we found that the differences between high and low latitude regions become more pronounced for X-rays with energies exceeding 20 keV (Figure 2). This distinction is likely caused by radiation belt electron precipitation. However, determining whether these X-rays are produced by auroral electrons or higher-energy electrons will require further in-depth research in future work. In future work, we will also consider the reviewer's suggestion to find suitable observations of auroral electrons that have eliminated its effect.

Minor comments:

Figure 2: These plots should be extended down to 40 km or so to show where the new ionization profile blends back into the background profile.

Also, it's not clear why the authors show both 1500 keV and 1 MeV, and in that order. Those energies seem too close to show any meaningful difference. Why not 100 keV, 300 keV, and 1 MeV?

Your suggestion is very helpful and has improved the clarity of our manuscript. We have implemented the following changes to Figures 2 and 3:

- Extended the altitude range down to 40 km to better illustrate where the new ionization profiles merge with the background profile.
- Replaced the previously similar energy values (1500 keV and 1 MeV) with a more informative set: 100 keV, 300 keV, and 1 MeV. This selection provides a clearer demonstration of the energy-dependent variations in electron penetration depths.

The results in Table 1 are a nice addition to the paper, but the authors should explain what "Moran's I" means to those who are unfamiliar with that method.

Moran's I is a spatial autocorrelation statistical method used to measure the degree of clustering or dispersion of data in space. We chose this method because it effectively quantifies the correlation between X rays, precipitated electrons and reflection height in the spatial distribution.

The values of Moran's I typically range from -1 to +1:

- Positive values (close to +1) indicate positive correlation.
- Negative values (close to -1) indicate negative correlation.
- Values close to zero indicate no apparent correlation.

We have revised Lines 275-276: "which is a spatial correlation statistical method and helpful in determining the correlation of different variables in the space. "

Reference:

Berger, M. J. and Seltzer, S. M.: Bremsstrahlung in the atmosphere, Journal of Atmospheric and Terrestrial Physics, 34, 85-108, https://doi.org/10.1016/0021-9169(72)90006-2, 1972.

Lehtinen, N. G., Bell, T. F., and Inan, U. S.: Monte Carlo simulation of runaway MeV electron breakdown with application to red sprites and terrestrial gamma ray flashes, Journal of Geophysical Research-Space Physics, 104, 24699-24712, 10.1029/1999ja900335, 1999.

Liao, L., Zhao, S., Li, Q., Dong, X., Lu, H., and Shen, X.: CSES Satellite Observation of Nightside Bremsstrahlung X-Ray Distributions Induced by Energetic Electron Precipitation, Journal of Geophysical Research: Space Physics, 130, e2024JA033700, https://doi.org/10.1029/2024JA033700, 2025.

Linzmayer, V., Němec, F., Santolík, O., and Kolmašová, I.: Lightning-Induced Energetic Electron Precipitation Observed in Long-Term DEMETER Spacecraft Measurements, Journal of Geophysical Research: Space Physics, 129, e2024JA032713, https://doi.org/10.1029/2024JA032713, 2024.

Voss, H. D., Imhof, W. L., Walt, M., Mobilia, J., Gaines, E. E., Reagan, J. B., Inan, U. S., Helliwell, R. A., Carpenter, D. L., Katsufrakis, J. P., and Chang, H. C.: Lightning-induced electron precipitation, Nature, 312, 740-742, 10.1038/312740a0, 1984.

Xu, W. and Marshall, R. A.: Characteristics of Energetic Electron Precipitation Estimated from Simulated Bremsstrahlung X-ray Distributions, Journal of Geophysical Research: Space Physics, 124, 2831-2843, https://doi.org/10.1029/2018JA026273, 2019.